Rayleigh-Taylor Instability for viscous thin gas films: Application to Critical Heat Flux and Minimum Film Boiling

Byoung Jae Kim [a*], Jong Hyuk Lee [a], Kyung Doo Kim [a]
[a]*Thermal-Hydraulics Safety Research Division, KAERI, Daejeon*
[*]*Corresponding author: byoungjae@kaeri.re.kr*

1. Introduction

Rayleigh-Taylor instability for two inviscid fluids has been widely used to develop the models for the prediction of critical and minimum heat fluxes since [1]. A historical review of the hydrodynamic theories of boiling is described in [2]. The average distance between rising bubbles for film boiling is governed by the most dangerous wavelength. The interface rising speed is determined by the most rapid growth rate. However, when the gas film becomes thin to the extent of creeping flow, the viscous force is dominant over the inertia force. In this case, the gas viscosity cannot be neglected. Thus, a question may be raised. Can the hydrodynamic models based on the inviscid flow analysis predict well the physical phenomena even for thin gas films? Is the gas film thick enough to neglect the wall effect?

The purpose of this study is to answer the above question. The effects of fluid viscosity and phase change are discussed in this study. Afterward, the critical heat flux and minimum film boiling are appreciated in view of thin viscous films. The existing critical heat flux models for saturated pool boiling on horizontal surfaces are modified to improve the prediction capability at elevated pressures.

2. Rayleigh-Taylor Instability

The two-dimensional configuration of Rayleigh-Taylor instability is depicted in Fig. 1. A lighter fluid (gas) is bounded by a heating wall and a semi-infinite heavier fluid (liquid) in the extent. In this chapter, the most dangerous wavelength (λ_d) and the most rapid growth rate (ω_d) are derived using four different analyses.

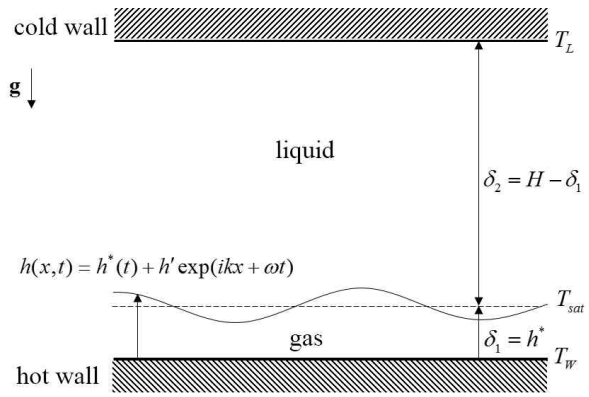

Fig. 1. Two-dimensional configuration of RT instability. A lighter fluid is beneath a heavier fluid

2.1 Inviscid Flow Analysis

The fluid viscosities are neglected in the classical inviscid flow analysis. The linear stability analysis for a small disturbance ($\sim \exp(ikx + \omega t)$) leads to the following dispersion relation:

$$\omega = \left(\frac{\Delta\rho g k - \sigma k^3}{\rho_1 \coth(k\delta_1) + \rho_2 \coth(k\delta_2)} \right)^{1/2}, \quad (1)$$

where ω , k , ρ , δ , σ , and g are the growth rate, wavenumber, fluid density, fluid layer thickness, surface tension, and gravitational acceleration, respectively. Subscripts 1 and 2 represent the lower and upper fluids, respectively, and $\Delta\rho = \rho_2 - \rho_1$ is the density difference. For a thick gas film beneath semi-infinite liquid, λ_d and ω_d can be obtained by equating $d\omega / dk$ to zero.

$$\lambda_d = 2\pi \left(3\sigma / \Delta\rho g\right)^{1/2} = \sqrt{3}\lambda_{c,\inf}, \quad (2)$$

$$\omega_d = \left(\frac{2}{3\sqrt{3}} \right)^{1/2} \left[\frac{(\Delta\rho g)^3}{\sigma(\rho_1 + \rho_2)^2} \right]^{1/4}, \quad (3)$$

where $\lambda_{c,\inf} = 2\pi(\sigma / \Delta\rho g)^{1/2}$ is the critical wavelength for two semi-infinite fluids. On the other hand, for thin gas layers ($k\delta_1 \to 0$), Eq. (1) goes over into

$$\omega \approx \left[\delta_1 (\Delta\rho g k^2 - \sigma k^4) / \rho_1 \right]^{1/2}. \quad (4)$$

From this, we obtain

$$\lambda_d = 2\pi \left(2\sigma / \Delta\rho g\right)^{1/2} = \sqrt{2}\lambda_{c,\inf}, \quad (5)$$

$$\omega_d = 0.5\Delta\rho g \left(\delta_1 / \rho_1 \sigma\right)^{1/2}. \quad (6)$$

Equation (1) was solved for a vapor film beneath semi-infinite water at the saturated conditions. Figure 2 shows the results. The abscissa is the gas film thickness divided by the capillary length ($l_c = (\sigma / \Delta\rho g)^{1/2}$). In Fig. 2, IF stands for the inviscid flow analysis. $\lambda_d / \lambda_{c,\inf}$ is no longer $\sqrt{3}$ for thin films, but is approaches $\sqrt{2}$. For minimum film boiling of water at atmospheric pressure, δ_1 is the order of 0.1 mm and l_c is estimated to 7.8 mm; δ_1 / l_c =0.0128. It is seen in Fig. 2 that $\lambda_d / \lambda_{c,\inf}$ is about $1.7 \approx \sqrt{3}$ for δ_1 / l_c =0.0128. [3] performed the inviscid flow analysis in a non-dimensional form, and arrived at the similar result. However, as a matter of fact, all the curves in Fig. 2 must be shifted rightward on the whole (see Fig 3 for a fully viscous flow analysis). Comparison of Fig. 2 with Fig. 3 will be discussed in section 2.3.

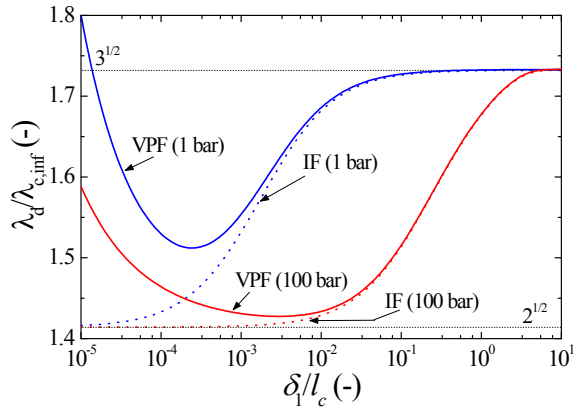

Fig. 2. Results of the inviscid flow analysis (IF) and the viscous potential flow analysis (VPF) for saturated properties of water and vapor

[4] incorporated the effect of phase change into R-T instability based on inviscid flow analysis. In his analysis, the base interface was set to be at rest without evaporation. This situation may occur in highly subcooled film boiling [5]. In the limit of the thin gas film beneath the semi-infinite liquid, the dispersion relation of [6] is approximated to (details are not described here)

$$\omega = \frac{\delta_l}{\alpha}(\Delta\rho g k^2 - \sigma k^4) \ . \qquad (7)$$

where $\alpha = K_l \Delta T_W / L\delta_l^2$ is a measure of heat and mass transfer at the interface (K : thermal conductivity, $\Delta T_W = T_W - T_{sat}$: wall superheat, L : latent heat). Equation (7) indicates $\lambda_d = \sqrt{2}\lambda_{c,\inf}$ no matter how evaporation is intensive, which is not correct. This prediction may be attributed to the fact that the viscosity is not included in the analysis.

2.2 Viscous Potential Analysis

In potential flow, the fluid velocity is described by the gradient of a scalar function (velocity potential). As a result, a potential flow is characterized by an irrotational velocity field. When the vorticity is zero (irrotational flow), the viscous term in the Navier-stokes equation is identically zero, but the viscous stresses are not zero [7]. In the stability analysis based on the viscous potential theory, tangential stresses are not considered but viscosity enters through normal stress balance at the interface, and the motion of fluid is governed by the Bernoulli's equation. This viscous potential flow analysis was applied to capillary instability by [8], and it was shown to be a better approximation of the exact solution than the classical inviscid model in view of the growth rate. The dispersion relation for Rayleigh-Taylor instability based on the viscous potential model was obtained by [9], and was modified by [10] to include the evaporation effect.

The dispersion relation given by [10] (not described here) was solved for the vapor film beneath the semi-infinite water, without phase change. Figure 2 compares the results with the classical inviscid analysis. For thick vapor films, there is almost no difference between the viscous potential analysis (VPF) and the classical inviscid analysis (IF). However, for VPF, λ_d increases unboundedly with decreasing the gas film thickness. This prediction is not correct. Therefore, the viscous potential flow analysis seems inappropriate for R-T instability for thin viscous film, in view of λ_d and ω_d .

2.3 Fully-Viscous Flow Analysis

An instability analysis for viscous fluids was made by [11]. Since his work is based on the complete Navier-Stokes equation, it is considered to be the exact solution. The dispersion relation for a gas layer bounded by a wall and semi-infinite liquid is described in Appendix 1. Figure 3 shows $\lambda_d / \lambda_{c,\inf}$ as a function of δ_l / l_c for saturated properties of water and vapor, which was obtained by numerically solving the dispersion relation Eq. (A.1) in Appendix 1. While $\lambda_d / \lambda_{c,\inf}$ asymptotically settles to $\sqrt{3}$ for thick films, it approaches $\sqrt{2}$ for the thin films.

Let us compare the curves in Fig. 3 with those in Fig. 2. On the whole, the curves in Fig. 3 are shifted rightward, compared to those in Fig. 2. Therefore, λ_d predicted by the inviscid flow analysis is higher than that by the viscous flow analysis. In particular, the movement of the curve is remarkable for the low pressure. For example, δ_l / l_c is estimated as 0.0128 for the minimum film boiling at atmospheric pressure. At this film thickness, $\lambda_d / \lambda_{c,\inf}$ is about $\sqrt{3}$ in Fig. 2, but it is close to $\sqrt{2}$ in Fig. 3. Moreover, since the vapor thickness decreases in increasing pressure, $\lambda_d / \lambda_{c,\inf}$ would be $\sqrt{2}$ at high pressures. A fully viscous flow analysis was also performed for pentane and Freon 133 at atmospheric pressure. For those fluids, $\lambda_d / \lambda_{c,\inf}$ fell below 1.45 when δ_l / l_c decreased to 0.1 (not provided here). However, since δ_l / l_c is estimated to be about 0.05 at minimum film boiling [3], $\lambda_d / \lambda_{c,\inf}$ would be $\sqrt{2}$.

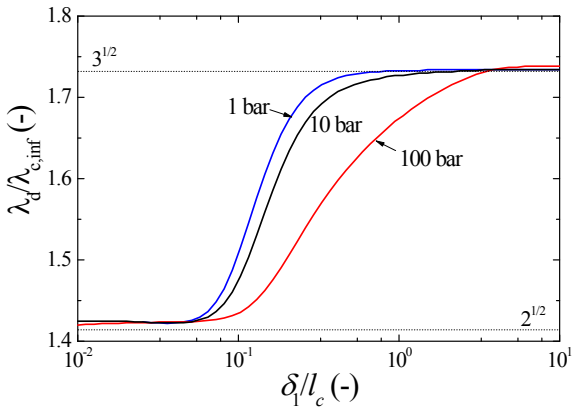

Fig. 3. Result of the fully viscous flow analysis for saturated properties of water and vapor

[12] included phage change in the stability analysis for two semi-infinite fluids with the same kinematic viscosity. [12] showed that there was a strong stabilizing effect arising from the coupling of viscosity and phase change. However, Ho's dispersion relation does not reduce to the form derived by [11] for the case of isothermal flow. [13] presented a more accurate dispersion relation for the same fluid configuration than [12]. No previous work has been found on the stability analysis for the case in which two fluids have different viscosities, their thicknesses are finite, and phage change takes place at the interface.

2.4 Thin Film Analysis Based on Lubrication Theory

According to a fully viscous flow analysis, the gas film is thin enough for flow to be viscous dominant. If the film is very thin, a parallel creeping flow can be assumed. However, the dispersion relation by the fully viscous flow analysis is still complicated to be solved analytically. A way to find a good solution is to use the lubrication theory for thin gas/liquid films. The motions of thin liquid films were extensively reviewed by [14] and [15]. The interface evolution of a thin gas film beneath semi-infinite liquid was investigated by [16], but without evaporation. [17] incorporated the evaporation effect into the lubrication approximation. However, the vapor thrust (or vapor recoil) at the interface was not considered. [18] included the vapor thrust effect for saturated film boiling, but discussion was limited to a specific condition near the critical pressure.

In Appendix 2, the lubrication equation is formulated considering the vapor thrust effect not only for saturated film boiling also for subcooled film boiling. The interface evolution equation is given by Eq. (A.11).

$$\frac{\partial h}{\partial t}=\frac{Q_1}{h}-\frac{Q_2}{H-h}-\frac{1}{12\mu_1}\left[h^3\left(\Delta\rho g h+\sigma h_{xx}+R\right)_x\right]_x \quad (8)$$

where

$$Q_1=K_1\Delta T_W/\rho_1 L\,, \quad (9a)$$

$$Q_2=K_2\Delta T_L/\rho_1 L\,, \quad (9b)$$

$$R=\frac{\rho_1}{\rho_2}\Delta\rho\left[\frac{Q_1^2}{h^2}-\frac{2Q_1Q_2}{h(H-h)}+\frac{Q_2^2}{(H-h)^2}\right]. \quad (9c)$$

$h=h(x,t)$ is the interface height hereafter. The first two terms on the right-hand side in Eq. (8) account for net inflow into the vapor film through the interface, and R takes charge of the vapor thrust effect.

An instability analysis is now performed. The liquid layer is much thicker than the gas layer such that $H-h\approx H$. Let $h=h^*$ be the interface height of a base state, which is spatially uniform but time-dependent. Since every order partial derivative of h^* with regard to x is zero, Eq. (8) becomes

$$\frac{\partial h^*}{\partial t}=\frac{Q_1}{h^*}-\frac{Q_2}{H}\,. \quad (10)$$

For saturated film boiling ($Q_2=0$), all of the heat conducted across the vapor layer goes into evaporation. In this case, h^* increases continuously with time since the right-hand side of Eq. (10) has a positive value. For subcooled film boiling ($Q_2\neq 0$), there exist a stationary solution. Initially, h^* may remain, increase, or decrease depending on the initial interface height, but it eventually attains a steady-state when the right side of Eq. (10) becomes zero.

Let us impose a small perturbation on the base state ($h'\ll h^*$).

$$h(x,t)=h^*(t)+h'\exp(ikx+\omega t)\,. \quad (11)$$

If the base state is time-dependent, the growth rate depends not only on the wavenumber but also on time. Substituting Eq. (11) into Eq. (8) and neglecting the products of small perturbed quantities ($h'h'\approx 0$),

$$\begin{aligned}&\frac{\partial h^*}{\partial t}+\frac{\partial(\omega t)}{\partial t}h'\exp(ikx+\omega t)\\&=\left[\frac{Q_1}{h^*}-\frac{Q_1}{h^{*2}}h'\exp(ikx+\omega t)\right]-\frac{Q_2}{H}\\&-\frac{h^{*3}}{12\mu_1}\left[\begin{array}{l}-\Delta\rho g k^2+\sigma k^4\\+\dfrac{\rho_1\Delta\rho}{\rho_2}\left(\dfrac{2Q_1^2}{h^{*3}}-\dfrac{2Q_1Q_2}{h^{*2}H}\right)k^2\end{array}\right]h'\exp(ikx+\omega t)\end{aligned}\,. \quad (12)$$

Equation (10) is subtracted from Eq. (12) to give

$$\frac{\partial(\omega t)}{\partial t}=-\frac{Q_1}{h^{*2}}+\frac{h^{*3}}{12\mu_1}\left[\begin{array}{l}\Delta\rho g k^2-\sigma k^4\\-\dfrac{\rho_1\Delta\rho}{\rho_2}\left(\dfrac{2Q_1^2}{h^{*3}}-\dfrac{2Q_1Q_2}{h^{*2}H}\right)k^2\end{array}\right]. \quad (13)$$

The growth rate is then computed as

$$\omega=\frac{1}{t}\int_0^t\left\{-\frac{Q_1}{h^{*2}}+\frac{h^{*3}}{12\mu_1}\left[\begin{array}{l}\Delta\rho g k^2-\sigma k^4\\-\dfrac{\rho_1\Delta\rho}{\rho_2}\left(\dfrac{2Q_1^2}{h^{*3}}-\dfrac{2Q_1Q_2}{h^{*2}H}\right)k^2\end{array}\right]\right\}dt \quad (14)$$

Unless the base state is time-dependent, ω is not a function of time. In this case,

$$\omega=-\frac{Q_1}{h^{*2}}+\frac{h^{*3}}{12\mu_1}\left[\begin{array}{l}\Delta\rho g k^2-\sigma k^4\\-\dfrac{\rho_1\Delta\rho}{\rho_2}\left(\dfrac{2Q_1^2}{h^{*3}}-\dfrac{2Q_1Q_2}{h^{*2}H}\right)k^2\end{array}\right] \quad (15)$$

Our main concern is placed on the most dangerous wavelength. In Eq. (14), the term $-Q_1/h^{*2}$ does not influence λ_d since Q_1 and h^* are independent of k. Thus, ω is maximized when the value in the square bracket in Eq. (14) has the largest value. Consequently, we can obtain the most dangerous wavelength as follows:

$$\lambda_d=2\pi\Big/\sqrt{\frac{\Delta\rho g}{2\sigma}\left(1-M_R\right)}\,, \quad (16a)$$

$$M_R=\frac{2\rho_1Q_1^2}{\rho_2 g h^{*3}}-\frac{2\rho_1Q_1Q_2}{\rho_2 g h^{*2}H}. \quad (16b)$$

This is the analytical expression for λ_d based on the lubrication approximation, which is valid not only for

saturated film boiling but also for subcooled film boiling. We call M_R the vapor thrust number. As h^* increases (but still thin enough for creeping flow) or the subcooling increases, the vapor thrust number reduces, and thus λ_d approaches $\sqrt{2}\lambda_{c,\inf}$. For $M_R \geq 1$, the present analysis is no longer valid and other theoretical analyses should be used. Figure 4 shows the vapor thrust number for saturated minimum film boiling of water ($Q_2 = 0$). The computation details will be described in section 3.2. As seen in Fig. 4, the vapor thrust number is much small than unity in the wide range of pressure, so that λ_d is $\sqrt{2}\lambda_{c,\inf}$ at the minimum film boiling point. However, the vapor thrust number may be important for high heat fluxes.

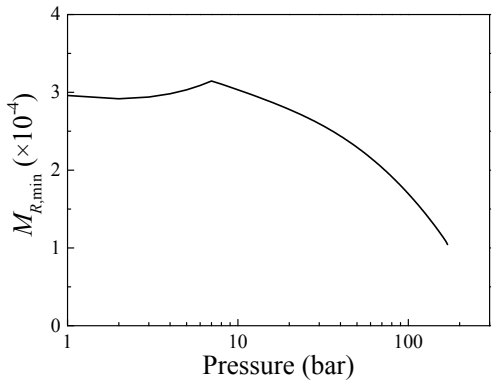

Fig. 4. Vapor thrust number for saturated minimum film boiling of water

3. Applications to Hydrodynamic Models

3.1 Critical Heat Flux

[1] laid the foundation of a hydrodynamic theory for critical and minimum heat fluxes in pool boiling on horizontal surfaces. Lienhard and his coworkers have supported Zuber`s model by extending the applicable range [19, 20]. Arguments for Zuber`s formulation are described in [2]. Another type of critical heat flux model in pool boiling was proposed by [21], that is, the liquid macro-layer dryout model. Later, [22] extended the applicable geometries and flow conditions. Very recently, [23] proposed a critical heat flux model based on the lift-off concept of the liquid macro-layer. The above critical heat flux models are limited to inviscid liquids for surfaces that are well wetted.

[1] postulated that for critical heat flux, vapor jets rise at the nodes of Taylor waves whose distance is λ. As a result, the following expression for critical heat flux was suggested.

$$q_{\max} = \frac{\pi}{16}\rho_1 L U_1 (1+\rho_1/\rho_2)^{0.5}, \quad (17)$$

$$U_1 = \sqrt{2\pi\sigma/\rho_1\lambda_H}, \quad (18)$$

The rising gas jet velocity (U_1) is expressed in terms of the critical wavelength (λ_H) by Kelvin-Helmholtz instability. His choice for λ_H was the critical wavelength for capillary waves on a circular jet, $\lambda_H = 2\pi R_j = 2\pi(\lambda/4) = \pi\lambda/2$, where R_j is the radius of a circular gas jet. If the distance between nodes of Taylor waves is expressed as $\lambda = \sqrt{\beta}\lambda_{c,\inf}$, Zuber`s formulation [1] can be rewritten as

$$q_{\max} = C\frac{\pi}{24}\rho_1^{1/2} L(\sigma\Delta\rho g)^{1/4}(1+\rho_1/\rho_2)^{1/2}, \quad (19)$$

$$C = 3/\left(2\pi\sqrt{\beta}\right)^{1/2}. \quad (20)$$

Zuber assumed that the wavelength fell between the critical wavelength ($\beta = 1$) and the most dangerous wavelength ($\beta = 3$). Thus, C varies between 0.909 and 1.197. He approximated the average value of C, 1.053, to unity. As a result, Eq. (19) becomes

$$q_{\max,Z} = 0.131\rho_1^{1/2} L(\sigma\Delta\rho g)^{1/4}(1+\rho_1/\rho_2)^{1/2}. \quad (21)$$

If λ is replaced with $\lambda_d = \sqrt{2}\lambda_{c,\inf}$ according to the result in the precedent chapter, C is computed to 1.006. It is interesting to note that this value leads to Eq. (21).

[20] noticed that Eq. (21) slightly underpredicted the experimental data. Thus, they chose $\lambda_H = \lambda_d = \sqrt{3}\lambda_{c,\inf}$ instead of $2\pi R_j$. As a result, Eq. (17) becomes

$$q_{\max,L} = 1.49\rho_1^{1/2} L(\sigma\Delta\rho g)^{1/4}(1+\rho_1/\rho_2)^{1/2}. \quad (22)$$

Again, when $\lambda_d = \sqrt{3}\lambda_{c,\inf}$ is replaced with $\lambda_d = \sqrt{2}\lambda_{c,\inf}$, We obtain newly

$$q_{\max} = 1.65\rho_1^{1/2} L(\sigma\Delta\rho g)^{1/4}(1+\rho_1/\rho_2)^{1/2}. \quad (23)$$

Meanwhile, [23] developed a critical heat flux model considering the lift-off of the liquid macro-layer. In their model, the width of the liquid macro-layer is determined by λ_d. With $\lambda_d = \sqrt{\beta}\lambda_{c,\inf}$, their expression becomes

$$q_{\max} = C\rho_1^{1/2} L(\sigma\Delta\rho g)^{1/4} \times(1+\rho_1/\rho_2)^{1/4}(\rho_1/\rho_2)^{1/10}, \quad (24)$$

$$C = (0.00341\pi/\beta)^{1/4}. \quad (25)$$

[23] used $\beta = 3$ based on the inviscid flow analysis, which yields $C = 0.2445$. Thus, Eq. (24) becomes

$$q_{\max,G} = 0.245\rho_1^{1/2} L(\sigma\Delta\rho g)^{1/4} \times(1+\rho_1/\rho_2)^{1/4}(\rho_1/\rho_2)^{1/10}. \quad (26)$$

The ratio of this model to Zuber`s model is $q_{\max,G}/q_{\max,Z} = 1.866(1+\rho_1/\rho_2)^{-1/4}(\rho_1/\rho_2)^{1/10}$, which indicates a larger increase in critical heat flux with increasing pressure than Zuber`s model. If $\beta = 2$ is used as a result of viscous films, we obtain newly

$$q_{\max} = 0.271\rho_1^{1/2} L(\sigma\Delta\rho g)^{1/4} \times(1+\rho_1/\rho_2)^{1/4}(\rho_1/\rho_2)^{1/10}. \quad (27)$$

The leading coefficient is increased by 11 % compared to Guan`s original model.

Only a small amount of experimental data is available for critical heat flux on large horizontal surfaces. The present modified models, Eqs. (23) and (27), are compared with experimental data for water in Fig. 5 and 6, respectively. Zuber`s correlation considerably underpredicts critical heat flux for elevated pressures. However, the present models predict critical heat flux more accurately in a wide range of pressure.

3.2 Minimum Film Boiling

λ_d and ω_d for minimum film boiling of water are investigated in this section. As seen in Eqs. (16a) and (16b), the most dangerous wavelength is affected by the vapor trust number M_R. Let $\Delta T_{\min}$ and $\delta_{\min}$ be the wall superheat and the vapor film thickness at the minimum film boiling point, respectively. In this section, M_R is evaluated for saturated minimum film boiling ($h^* = \delta_{\min}$ and $Q_2 = 0$).

$$M_{R,\min} = \frac{2\rho_1 Q_1^2}{\rho_2 g h^{*3}} = \frac{2(K_1 \Delta T_{\min})^2}{\rho_1 \rho_2 g L^2 \delta_{\min}^3}. \qquad (28)$$

To evaluate $M_{R,\min}$, $\Delta T_{\min}$ and $\delta_{\min}$ must be determined.

[24] developed a $\Delta T_{\min}$ correlation for horizontal cylinders from the extensive experimental data sources. The correlation covers the full range of pressure up to the critical pressure. He stated that $\Delta T_{\min}$ is not sensitive to surface configuration and dimensions. [25] measured $\Delta T_{\min}$ for various horizontal flat surfaces, but the test pressures were not very high (up to 12 bar). Figure 7 shows the variation of $\Delta T_{\min}$ with saturation pressure, where Yao` data points are for a stainless steel surface. It is shown that $\Delta T_{\min}$ does not vary significantly in a low pressure range. As a first approximation, $\Delta T_{\min}$ is 150 °C in a pressure range of 1~12 bar in [25]. The maximum liquid superheat (T_{ms}) can be used to set $\Delta T_{\min}$ at high pressures. The maximum liquid superheat was computed by $T_{ms} = \left[0.905 + 0.095(T_{sat}/T_{cr})^8\right] T_{cr}$ in terms of Kelvin [26]. It is interesting to note that $T_{ms} - T_{sat}$ matches Nishio`s predictions well at high pressures.

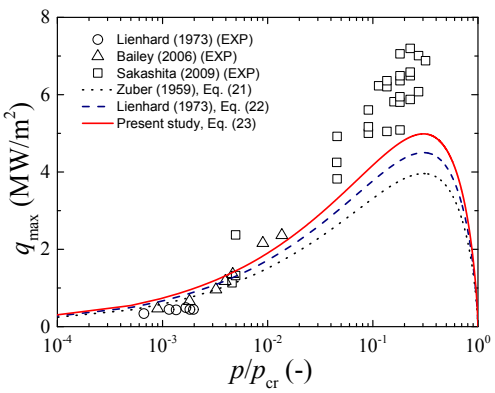

Fig. 5. Comparison of the present critical heat flux model, Eq. (23), with experimental data for water

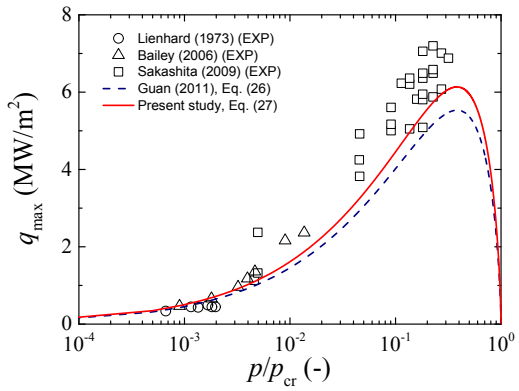

Fig. 6. Comparison of the present critical heat flux model, Eq. (27), with experimental data for water

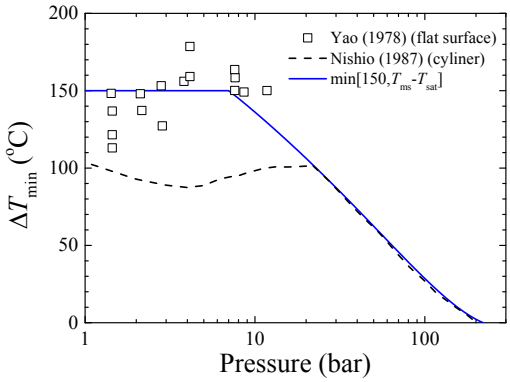

Fig. 7. Wall superheat for minimum film boiling of water on horizontal flat/cylinder surfaces

$\Delta T_{\min}$ was set to the minimum value between 150 °C and $T_{ms} - T_{sat}$ for calculating $M_{R,\min}$.

The minimum vapor film thickness was computed by $\delta_{\min} = K_1 / H_{\min}$ through a simple conduction equation, where $H_{\min}$ is the heat transfer coefficient. The most widely used correlations for the heat transfer coefficient in film boiling on horizontal surfaces are those developed by [27] and [3]. A number of numerical simulations verified that these two correlations can predict the heat transfer coefficient with acceptable accuracy even at high pressures [28-33]. It is also known that the correlations for fully developed film boiling can be applied even to minimum film boiling. Berenson`s correlation was used to determine $H_{\min}$.

$$H_{\min} = 0.425\left[\frac{k_l^3 L \rho_l \Delta\rho g}{\mu_l \Delta T_{\min}\sqrt{\sigma/\Delta\rho g}}\right]^{1/4}. \qquad (29)$$

For minimum film boiling, vapor properties at the mean vapor film temperature are not very different from those at the saturation temperature. Therefore, vapor properties at the saturation temperature were used to evaluate the heat transfer coefficient. Figure 4 shows that M_R is much small than unity in a wide range of pressure. Consequently, the vapor thrust effect can be neglected so that λ_d is $\sqrt{2}\lambda_{c,\inf}$ for minimum film boiling.

Next, the most rapid growth rate is discussed. Neglecting the vapor thrust effect in Eq. (14), we can write, for saturated minimum film boiling,

$$\omega = \frac{1}{t}\int_0^t \left[-\frac{Q_1}{h^{*2}} + \frac{h^{*3}}{12\mu_1}(\Delta\rho g k^2 - \sigma k^4) \right] dt \,. \quad (30)$$

The growth rate is determined by two contributions. At the initial height $h^* = \delta_{\min}$, Q_1 / h^{*2} may be dominant over $h^{*3}(\Delta\rho g k^2 - \sigma k^4)/12\mu_1$; the interface grows uniformly. However, the latter term increases rapidly as the interface grows while the former term diminishes. Therefore, the interface growth would be governed by the latter term during the most period until the bubble detaches from the wall. This behavior is also seen in numerical simulations by [34]. For this reason, the growth rate can be approximated as

$$\omega \approx \frac{1}{t}\int_0^t \left[\frac{h^{*3}}{12\mu_1}(\Delta\rho g k^2 - \sigma k^4) \right] dt \,. \quad (31)$$

If the growth rate is assumed to be constant in time, the most rapid growth rate becomes

$$\omega_d = \frac{h^{*3}(\Delta\rho g)^2}{48\mu_1\sigma} = \frac{\delta_{\min}^3(\Delta\rho g)^2}{48\mu_1\sigma} \,. \quad (32)$$

Finally, the minimum heat flux is discussed. [1] proposed the minimum heat flux correlation taking the following form:

$$q_{\min} = C_{\min}\rho_1 L \omega_d \lambda_d \,. \quad (33)$$

The coefficient $C_{\min}$ depends on the bubble diameter at breakoff, the release frequency, and the bubble spacing. Zuber substituted Eqs. (2) and (3) into Eq. (33) to obtain

$$q_{\min} = C\rho_1 L \left[\frac{\sigma\Delta\rho g}{(\rho_1 + \rho_2)^2} \right]^{1/4} \,. \quad (34)$$

He suggested the coefficient $C = 0.176$ for the semi-infinite vapor film. [27] related C to the initial vapor film thickness, and determined $C = 0.091$ from the experimental data at atmospheric pressure. [25] found that Berenson`s model works at only very low pressure (2 bar or less), and that it overpredicts unrealistically minimum heat flux at high pressures. A totally theoretical expression for constant C may not be possible unless the initial vapor film thickness is determined theoretically.

Substituting $\lambda_d = \sqrt{2}\lambda_{c,\inf}$ and $\omega_d = \delta_{\min}^3(\Delta\rho g)^2 / 48\mu_1\sigma$ (Eq. 32) into Eq. (33),

$$q_{\min} = \frac{\pi\sqrt{2}}{24} C_{\min} \frac{\rho_1 \Delta\rho g L \delta_{\min}^3}{\mu_1} \sqrt{\frac{\Delta\rho g}{\sigma}} \,. \quad (35)$$

Equating Eq. (35) to $K_1\Delta T_{\min} / \delta_{\min}$, we obtain the following:

$$\delta_{\min} = \left[\frac{24}{\pi\sqrt{2}C_{\min}} \right]^{1/4} \left[\frac{\mu_1 K_1 \Delta T_{\min}}{L\rho_1\Delta\rho g} \sqrt{\frac{\sigma}{\Delta\rho g}} \right]^{1/4} \,. (36)$$

It is interesting to compare the above with the vapor film thickness correlation by [27].

$$\delta_1 = 2.35 \left[\frac{\mu_1 K_1 \Delta T_W}{L\rho_1\Delta\rho g} \sqrt{\frac{\sigma}{\Delta\rho g}} \right]^{1/4} \,. \quad (37)$$

Equations (36) and (37) become identical if $(24/\pi\sqrt{2}C_{\min})^{1/4} = 2.35$. However, λ_d is relative to $\delta_1^{0.5}$ for thin gas films according to the inviscid flow analysis (Eq. (6)), which leads to an unrealistic vapor film thickness model.

4. Conclusions

Four types of Rayleigh-Taylor instability analyses have been applied to thin gas films. In particular, the dispersion relation including phase change was derived based on the lubrication approximation. The evaporation effect was shown to be negligible to find the most dangerous wavelength and the most rapid growth rate. As a result, it was shown that $\lambda_d = 2\pi\sqrt{2\sigma/\Delta\rho g}$ should be used for the most dangerous wavelength for thin vapor films. This value was used to modify the existing critical heat flux for saturated pool boiling on horizontal surfaces. The modified correlations showed good predictions in the wide rate of pressure. Moreover, the thin vapor film analysis correctly led to the expression for the vapor film thickness at minimum film boiling, which is consistent with the well-known existing correlation. The question raised in introduction is now answered. If the viscosity effect is neglected for thin gas films, the most dangerous wavelength and the most rapid growth rate are incorrectly predicted. Therefore, the viscous flow analysis must be performed than the inviscid flow analysis.

Acknowledgement

This work was supported by the Nuclear Power Technology Development Program of the Korea Institute of Energy Technology Evaluation and Planning (KETEP) grant funded by the Korea Government Ministry of Knowledge Economy (MKE). This work was also supported by the Nuclear Safety Research Center Program of the KORSAFe grant (Grant Code 1305011) funded by Nuclear Safety and Security Commission of the Korean government.

References

1. Zuber, N., *Hydrodynamic aspects of boiling heat transfer*. 1959, UCLA.
2. Lienhard, J.H. and L.C. Witte, *An Historical Review of the Hydrodynamic Theory of Boiling*, in *Reviews in Chemical Engineering*. 1985. p. 187.
3. Klimenko, V.V., *Film boiling on a horizontal plate — new correlation.* International Journal of Heat and Mass Transfer, 1981. **24**(1): p. 69-79.
4. Hsieh, D.Y., *Effects of Heat and Mass Transfer on Rayleigh-Taylor Instability.* Journal of Basic Engineering, 1972. **94**(1): p. 156-160.

5. Abbassi, A. and R.H.S. Winterton, *The non-boiling vapour film.* International Journal of Heat and Mass Transfer, 1989. **32**(9): p. 1649-1655.
6. Hsieh, D.Y., *Interfacial stability with mass and heat transfer.* Physics of Fluids (1958-1988), 1978. **21**(5): p. 745-748.
7. Joseph, D.D. and T.Y. Liao, *Potential flows of viscous and viscoelastic fluids.* Journal of Fluid Mechanics, 1994. **265**: p. 1-23.
8. Funada, T. and D.D. Joseph, *Viscous potential flow analysis of capillary instability.* International Journal of Multiphase Flow, 2002. **28**(9): p. 1459-1478.
9. Joseph, D.D., J. Belanger, and G.S. Beavers, *Breakup of a liquid drop suddenly exposed to a high-speed airstream.* International Journal of Multiphase Flow, 1999. **25**(6–7): p. 1263-1303.
10. Awasthi, M.K. and G.S. Agrawal, *Viscous potential flow analysis of Rayleigh-Taylor instability with heat and mass transfer.* International Journal of Applied Mathematics and Mechanics, 2011. **7**(12): p. 73-84.
11. Chandrasekhar, S., *Hydrodynamic and Hydromagnetic Stability*. 1961: Dover Publications.
12. Ho, S.-P., *Linear Rayleigh-Taylor stability of viscous fluids with mass and heat transfer.* Journal of Fluid Mechanics, 1980. **101**(01): p. 111-127.
13. Adham-Khodaparast, K., M. Kawaji, and B.N. Antar, *The Rayleigh–Taylor and Kelvin–Helmholtz stability of a viscous liquid–vapor interface with heat and mass transfer.* Physics of Fluids (1994-present), 1995. **7**(2): p. 359-364.
14. Oron, A., S.H. Davis, and S.G. Bankoff, *Long-scale evolution of thin liquid films.* Reviews of Modern Physics, 1997. **69**(3): p. 931-980.
15. Craster, R.V. and O.K. Matar, *Dynamics and stability of thin liquid films.* Reviews of Modern Physics, 2009. **81**(3): p. 1131-1198.
16. Yiantsios, S.G. and B.G. Higgins, *Rayleigh–Taylor instability in thin viscous films.* Physics of Fluids A: Fluid Dynamics (1989-1993), 1989. **1**(9): p. 1484-1501.
17. Panzarella, C.H., S.H. Davis, and S.G. Bankoff, *Nonlinear dynamics in horizontal film boiling.* Journal of Fluid Mechanics, 2000. **402**: p. 163-194.
18. Tomar, G., et al., *Multimode analysis of bubble growth in saturated film boiling.* Physics of Fluids (1994-present), 2008. **20**(9): p. -.
19. Lienhard, J.H. and V.K. Dhir, *Hydrodynamic Prediction of Peak Pool-boiling Heat Fluxes from Finite Bodies.* Journal of Heat Transfer, 1973. **95**(2): p. 152-158.
20. Lienhard, J.H. and V.K. Dhir, *Extended hydrodynamic theory of the peak and minimum pool boiling heat fluxes*. 1973.
21. Katto, Y. and S. Yokoya, *Principal mechanism of boiling crisis in pool boiling.* International Journal of Heat and Mass Transfer, 1968. **11**(6): p. 993-1002.
22. Haramura, Y. and Y. Katto, *A new hydrodynamic model of critical heat flux, applicable widely to both pool and forced convection boiling on submerged bodies in saturated liquids.* International Journal of Heat and Mass Transfer, 1983. **26**(3): p. 389-399.
23. Guan, C.-K., J.F. Klausner, and R. Mei, *A new mechanistic model for pool boiling CHF on horizontal surfaces.* International Journal of Heat and Mass Transfer, 2011. **54**(17–18): p. 3960-3969.
24. Nishio, S., *Prediction technique for minimum-heat-flux (MHF)-point condition of saturated pool boiling.* International Journal of Heat and Mass Transfer, 1987. **30**(10): p. 2045-2057.
25. Yao, S.-c. and R.E. Henry, *An Investigation of the Minimum Film Boiling Temperature on Horizontal Surfaces.* Journal of Heat Transfer, 1978. **100**(2): p. 260-267.
26. Lienhard, J.H., *Correlation for the limiting liquid superheat.* Chemical Engineering Science, 1976. **31**(9): p. 847-849.
27. Berenson, P.J., *Film-Boiling Heat Transfer From a Horizontal Surface.* Journal of Heat Transfer, 1961. **83**(3): p. 351-356.
28. Juric, D. and G. Tryggvason, *Computations of boiling flows.* International Journal of Multiphase Flow, 1998. **24**(3): p. 387-410.
29. Agarwal, D.K., et al., *Planar Simulation of Bubble Growth in Film Boiling in Near-Critical Water Using a Variant of the VOF Method.* Journal of Heat Transfer, 2004. **126**(3): p. 329-338.
30. Esmaeeli, A. and G. Tryggvason, *Computations of film boiling. Part II: multi-mode film boiling.* International Journal of Heat and Mass Transfer, 2004. **47**(25): p. 5463-5476.
31. Son, G. and V.K. Dhir, *Numerical Simulation of Saturated Film Boiling on a Horizontal Surface.* Journal of Heat Transfer, 1997. **119**(3): p. 525-533.
32. Son, G. and V.K. Dhir, *Numerical Simulation of Film Boiling Near Critical Pressures With a Level Set Method.* Journal of Heat Transfer, 1998. **120**(1): p. 183-192.
33. Guo, D.Z., et al., *Phase Change Heat Transfer Simulation for Boiling Bubbles Arising from a Vapor Film by the VOSET Method.* Numerical Heat Transfer, Part A: Applications, 2011. **59**(11): p. 857-881.
34. Tomar, G., et al., *Numerical simulation of bubble growth in film boiling using a coupled level-set and volume-of-fluid method.* Physics of Fluids (1994-present), 2005. **17**(11): p. -.
35. Banerjee, D. and V.K. Dhir, *Study of Subcooled Film Boiling on a Horizontal Disc: Part I—Analysis.* Journal of Heat Transfer, 2000. **123**(2): p. 271-284.

Appendix 1

[16] provided the dispersion relation for a gas film bounded by a wall and semi-infinite liquid. The dimensionless parameters are defined as follows:

$\alpha = \delta_1 k$, (dimensionless wavenumber)

$c = \omega\mu_1 / \Delta\rho g\delta_1$, (dimensionless growth rate)

$m = \mu_2 / \mu_1$, (viscosity ratio)

$r = \rho_2 / \rho_1$, (density ratio)

$F = \rho_1\Delta\rho g\delta_1^3 / \mu_1^2$, (relative magnitude of gravity forces to viscous forces)

$B = \Delta\rho g\delta_1^2 / \sigma$, (Bond number)

and

$p = \sqrt{\alpha^2 + Fc}$,

$q = \sqrt{\alpha^2 + rFc/m}$,

$T = (\alpha - \alpha^3 B^{-1}) / c$.

The linear stability analysis for the Navier Stokes equation yields the following dispersion relation:

$$A_1B_1 + A_2B_2 + A_3B_3 + A_4B_4 + A_5B_5 + A_6 = 0 , \quad (A.1)$$

where

$$A_1 = (\alpha^2 - p^2)\left[T - mq(\alpha + q)\right],$$
$$A_2 = \left[T - m(\alpha^2 + q^2)\right]m(\alpha + q) + 2m(1-m)\alpha^2(q - \alpha)$$
$$A_3 = m(\alpha^2 - p^2)p(\alpha + q),$$
$$A_4 = (\alpha^2 + p^2)^2 + 2m\alpha p^2(q - \alpha),$$
$$A_5 = 2\alpha^2 p\left[m(q - \alpha) + 2\alpha\right],$$
$$A_6 = 2\alpha p(\alpha^2 + p^2)\left[m(q - \alpha) + 2\alpha\right],$$

and

$$B_1 = \alpha\cosh\alpha\sinh p - p\sinh\alpha\cosh p,$$
$$B_2 = 2\alpha p(1 - \cosh\alpha\cosh p) + (\alpha^2 + p^2)\sinh\alpha\sinh p$$
$$B_3 = p\cosh\alpha\sinh p - \alpha\sinh\alpha\cosh p$$
$$B_4 = \alpha\sinh\alpha\sinh p - p\cosh\alpha\cosh p,$$
$$B_5 = p\sinh\alpha\sinh p - \alpha\cosh\alpha\cosh p.$$

Equation (A.1) relates the dimensionless growth rate (c) to the dimensionless wavenumber (α).

Appendix 2

In this appendix, an interface evolution equation is derived considering evaporation. In general, the interface evolution equation is derived through scaling analysis. Here, the interface evolution is formulated in a simple manner. The vapor is assumed to be incompressible. Take a small 2D control volume in a vapor film (Fig. 8). Let $\mathbf{v}_i$, $\mathbf{v}_{1i}$, and $\mathbf{v}_{2i}$ denote the interface velocity, the vapor velocity at the interface, and liquid velocity at the interface, respectively. The interface varies slowly in space. $\mathbf{v}_{1i}$ is assumed to be nearly uniform within the interval Δx. Unless the evaporation is quite intensive, the flow will be nearly parallel to the wall. According to numerical simulations for horizontal film boiling [35], the vapor flow is parallel to the wall in most regions.

From the conservation of mass ($Q_{in}, Q_{out1}, Q_{out2}$: volume flow rates, m^2/s),

$$\mathbf{v}_{1i}\cdot\mathbf{n}_1 = \frac{1}{12\mu_1}\left[h^3(p_1)_x\right]_x. \qquad \text{(A.2)}$$

The fraction 1/12 is because a Poiseuille flow is assumed. If the shear stress at the interface had been negligible, the fraction would be replaced by 1/3. The unbalanced energy transfer at the interface leads to vapor generation.

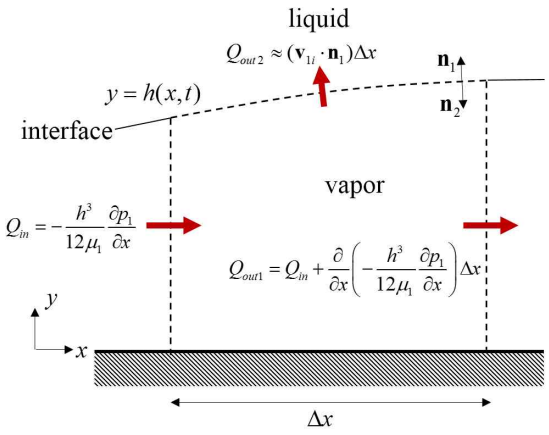

Fig. 8. Control volume in a thin vapor film

It is assumed that heat transfer occurs in liquid due to the steady conduction only. Thus,

$$\frac{K_1\Delta T_W}{h} - \frac{K_2\Delta T_L}{H-h} = L\left[-\rho_1(\mathbf{v}_{1i} - \mathbf{v}_i)\cdot\mathbf{n}_1\right], \quad \text{(A.3)}$$

where K, L, $\Delta T_W = T_W - T_{sat}$, and $\Delta T_L = T_{sat} - T_L$ are the fluid thermal conductivity, latent heat, wall superheat, and liquid subcooling, respectively. Equation (A.3) is arranged to give

$$\mathbf{v}_i\cdot\mathbf{n}_1 = \frac{K_1\Delta T_W}{\rho_1 L}\frac{1}{h} - \frac{K_2\Delta T_L}{\rho_1 L}\frac{1}{H-h} + \mathbf{v}_{1i}\cdot\mathbf{n}_1. \quad \text{(A.4)}$$

Substituting for $\mathbf{v}_{1i}\cdot\mathbf{n}_1$ from Eq. (A.2), we obtain

$$\mathbf{v}_i\cdot\mathbf{n}_1 = \frac{K_1\Delta T_W}{\rho_1 L}\frac{1}{h} - \frac{K_2\Delta T_L}{\rho_1 L}\frac{1}{H-h} + \frac{1}{12\mu_1}\left[h^3(p_1)_x\right]_x \quad \text{(A.5)}$$

Because the interface is nearly parallel to the wall, the right-hand side can be approximated to $\mathbf{v}_i\cdot\mathbf{n}_1 \approx \partial h/\partial t$. Defining $Q_1 = K_1\Delta T_W/\rho_1 L$ and $Q_2 = K_2\Delta T_L/\rho_1 L$, Eq. (A.5) can be recast into

$$\frac{\partial h}{\partial t} = \frac{Q_1}{h} - \frac{Q_2}{H-h} + \frac{1}{12\mu_1}\left[h^3(p_1)_x\right]_x. \quad \text{(A.6)}$$

For an isothermal flow ($Q_1 = Q_2 = 0$), the pressure gradient term is expressed by $(p_1)_x = (-h\Delta\rho g - \sigma h_{xx})_x$ owing to the normal pressure balance condition at the interface ([Yiantsios and Higgins [16]]. When phage change takes place, however, the term should be modified to include the vapor thrust effect.

$$(p_1)_x = \left[-h\Delta\rho g - \sigma h_{xx} - \dot{m}_1(\mathbf{v}_{1i} - \mathbf{v}_{2i})\cdot\mathbf{n}_1\right]_x, \quad \text{(A.7)}$$

where $\dot{m}_1 = \rho_1(\mathbf{v}_{1i} - \mathbf{v}_i)\cdot\mathbf{n}_1$ is the mass efflux. The vapor thrust term in Eq. (A.7) can be expressed as

$$\dot{m}_1(\mathbf{v}_{1i} - \mathbf{v}_{2i})\cdot\mathbf{n}_1 = \frac{\Delta\rho}{\rho_1\rho_2}\dot{m}_1^2, \quad \text{(A.8)}$$

by the conservation of mass. The vapor generation rate per unit interface area is given by

$$-\dot{m}_1 = \frac{K_1\Delta T_W}{Lh} - \frac{K_2\Delta T_L}{L(H-h)} = \rho_1\left(\frac{Q_1}{h} - \frac{Q_2}{H-h}\right). \quad \text{(A.9)}$$

Upon substituting the above into Eq. (A.8), we obtain

$$R = \dot{m}_1(\mathbf{v}_{1i} - \mathbf{v}_{2i})\cdot\mathbf{n}_1 = \frac{\rho_1}{\rho_2}\Delta\rho\left[\frac{Q_1^2}{h^2} - \frac{2Q_1Q_2}{h(H-h)} + \frac{Q_2^2}{(H-h)^2}\right]. \quad \text{(A.10)}$$

Consequently, using the relations by Eqs. (A.7) and (A.17), Eq. (A.13) becomes

$$\frac{\partial h}{\partial t} = \frac{Q_1}{h} - \frac{Q_2}{H-h} - \frac{1}{12\mu_1}\left[h^3(h\Delta\rho g + \sigma h_{xx} + R)_x\right]_x. \quad \text{(A.11)}$$

This is the interface evolution equation for thin viscous gas film including the phase change effect.